

Exsolution in Ferromagnesian Olivine of the Divnoe Meteorite

Michail I. Petaev and Adrian J. Brearley

Ferromagnesian olivine, one of the most common minerals in the solar system, has been widely regarded as a continuous solid solution, although several thermodynamic analyses have suggested the possibility of a miscibility gap at low temperatures. Natural ferromagnesian olivine from the Divnoe meteorite contains compositionally different exsolution lamellae, providing direct evidence for the existence of a miscibility gap in iron-magnesium olivine solid solutions.

Ferromagnesian olivine, $(\text{Mg,Fe})_2\text{SiO}_4$, is one of the most common minerals in the solar system. Compositionally it is a solid solution of the two end-members forsterite (Mg_2SiO_4) and fayalite (Fe_2SiO_4), with minor amounts of other elements such as Mn and Ca. The relatively simple composition and abundance of olivine has led to the widespread application of geothermobarometers with mineral equilibria involving olivine to understand geological processes in the Earth and extraterrestrial bodies. Correct application of these equilibria to rocks requires an understanding of the mixing properties of $(\text{Fe,Mg})_2\text{SiO}_4$ solid solutions, which are widely regarded as continuous (1, 2), although small positive deviations from ideality have been reported (3–5). In a recent thermodynamic analysis of phase relations in the system $\text{Mg}_2\text{SiO}_4\text{-Fe}_2\text{SiO}_4\text{-SiO}_2$, Sack and Ghiorso (6) predicted that olivine should show such larger deviations from ideality which, if true, profoundly affect geothermobarometry with this mineral. In addition, such nonideal behavior would be expected to result in exsolution of ferromagnesian olivine at temperatures less than 340°C if equilibrium can be achieved. Wisler and Wood (7) have questioned these predictions, on the basis of an experimental study which shows that although olivine solid solutions show positive deviations from ideality, the excess mixing energies are not of sufficient magnitude to result in exsolution. However, all the experimental data on olivine solid solutions have been obtained at high temperatures, and the uncertainties are rather large, so any of the mixing parameters proposed would fit them. Exsolution in olivine is predicted to occur at temperatures too low to permit equilibration to occur in reasonable experimental time scales, so that the observation of naturally exsolved olivine grains would contribute direct evidence to the existence of a miscibility gap in Fe-Mg olivine solid solu-

tions. Here we report on the discovery of such exsolution in ferromagnesian olivine grains in the Divnoe meteorite.

The Divnoe meteorite is a granoblastic, olivine-rich primitive achondrite whose textural and mineralogical characteristics suggest that it recrystallized extensively during slow cooling from $\sim 1000^\circ$ to $\sim 500^\circ\text{C}$ (8). Olivine grains in this meteorite show a lamellar appearance in back-scattered electron (BSE) images, caused by minor micrometer-scale chemical variations in Fe, Mg, and Mn contents between adjacent lamellae (8, 9). In some olivine grains, these variations are superimposed on a larger-scale compositional zoning. We studied 10 grains of lamellar olivine in detail by electron probe microanalysis (EPMA) and optical microscopy, and two of these by

transmission electron microscopy (TEM) (10).

The grains display slightly different lamellar structures, as shown in Fig. 1. We found the typical (ordinary) lamellar structure in BSE images, consisting of a regular pattern of alternating light (Fe-rich) and dark (Fe-poor) lamellae up to some tens of micrometers in thickness (Fig. 1A), in many grains, but only grain #1 also displays a clear lamellar structure by transmitted light (Fig. 1B). Some grains are composed of diffuse light and dark areas that contain bright (Fe-enriched), lens-shaped lamellae decorated by dark, irregular domains (Fig. 1C). A grain having both ordinary and lens-shaped lamellae was also observed (Fig. 1D).

The olivine grains studied are essentially free of minor elements (Ti, Al, Cr, Ni, Ca, Na), other than Mn (0.24 to 0.60% by weight), and are $\text{Fa}_{22.8-29.1}$ (Fa, mole percent) in composition. In spite of the different appearances of the grains, the compositional variations among lamellae display similar patterns in all the grains, including a strong correlation between Fe and Mn contents (11). Although the compositional ranges of Fe-poor and Fe-rich lamellae for all grains overlap, in any given grain the differences between the lamellae that are richest and poorest in Fe are similar (Table 1), which is suggestive of their formation by an equilibrium process. To better resolve

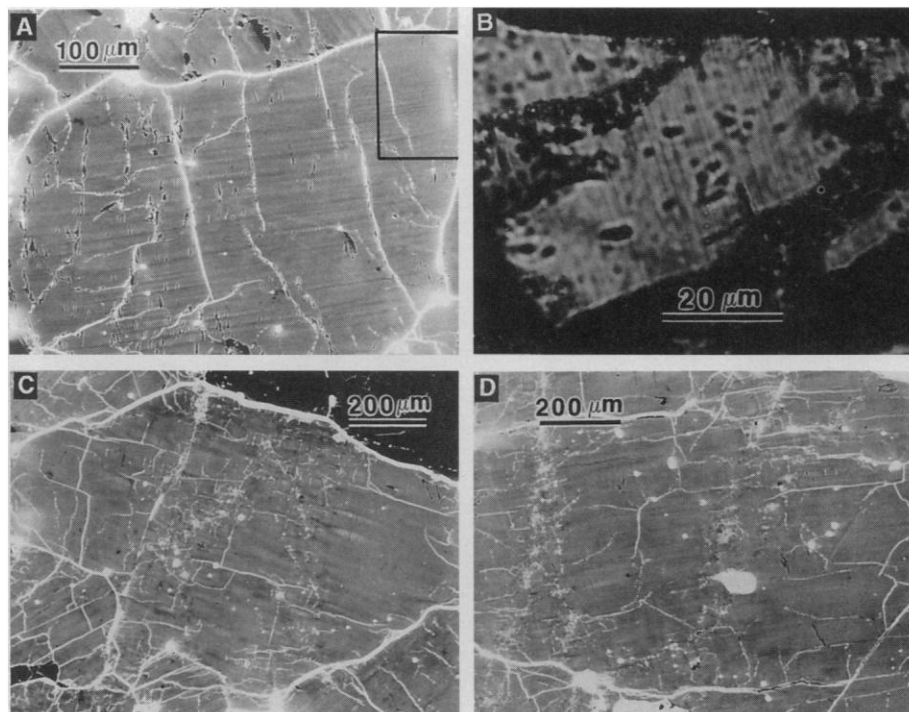


Fig. 1. Structures of olivine grains. (A) Ordinary lamellar structure in grain #1, BSE image. Light gray, Fe-rich areas; dark gray, Fe-poor areas; white, veins and inclusions of opaque minerals, mainly troilite. Marked inset is shown in (B). (B) Lamellar structure in grain #1, transmitted light. (C) Lens-shaped lamellae in grain #6, BSE image. (D) Mixed lamellar structure in grain #3, BSE image.

M. I. Petaev, Harvard-Smithsonian Center for Astrophysics, Cambridge, MA 02138, USA.
A. J. Brearley, Institute of Meteoritics, Department of Earth and Planetary Sciences, University of New Mexico, Albuquerque, NM 87131, USA.

the widths and chemical compositions of lamellae, we performed fine-scale EPMA step traverses of several ordinary lamellar grains. One of the traverses is shown in Fig. 2. We found that some thick, light, diffuse lamellae seen in the BSE image consist of several thinner lamellae a few micrometers wide. Compositional variations along the traverse describe a sine curve, with wavelength varying from a few micrometers to $\sim 5 \mu\text{m}$.

TEM studies of one grain containing ordinary lamellae (Fig. 3A) show that this microstructure is not due to the presence of lamellae of a second phase such as pyroxene or amphibole intergrown with the olivine. TEM imaging and electron diffraction analysis show that the grain consists entirely of crystalline olivine with an extremely high density of dislocations, typically concentrated in narrow, discontinuous bands, parallel to (010). This is the only orientation of dislocations observed in this sample. These dislocation arrays define the type of lamellar microstructure seen in transmitted light, but there are no clear interfaces between adjacent lamellae. The typical wavelength of these lamellae is 0.1 to 0.2 μm , substantially less than the widths of compositional lamellae observed by BSE imaging. Analytical TEM shows that the dislocation arrays do not necessarily correspond to boundaries between compositionally dis-

tinct lamellae, but analyses carried out at different points within a grain do show compositional differences that are comparable with those determined by EPMA (Table 1). An olivine grain containing both ordinary and lens-shaped lamellae (Fig. 3B) has a somewhat different microstructure than that just described. First, dislocation arrays are much less common and the dislocation density is lower. Second, the grain, at least locally, contains clear lamellae ($\sim 2 \mu\text{m}$ in width) along (010), separated by well-defined interfaces that are decorated by dislocations. Analytical TEM has confirmed that these lamellae differ compositionally by 1.0 to 1.5 mol% Fa. No zoning is detectable within or across lamellae, indicating equilibrium compositions.

The structural and compositional data presented above suggest that the lamellar structure in these olivine grains was produced by an exsolution process. Exsolution can proceed by three different mechanisms: heterogeneous nucleation, homogeneous nucleation, and spinodal decomposition (12). Because both Fe-rich and Fe-poor phases in the Divnoe olivine have the same structure and only a small difference in

composition (2 to 4 mol% Fa), heterogeneous nucleation does not seem to be required. Homogeneous nucleation could have produced the microstructure in grain #3, where there are clear interfaces between lamellae that are slightly different in composition. The ordinary lamellar grains with diffuse compositional lamellae could have been formed by spinodal decomposition, which induces compositional waves in a mineral grain but does not result in the formation of interfaces between compositionally different lamellae. However, compositional differences between adjacent lamellae do produce elastic strain in the exsolved crystals. The release of accumulated strain energy, which might have been triggered by collisional impacts in space, could have produced the observed dislocation arrays in olivine crystals.

Varying, but long wavelengths of spinodal decomposition in the Divnoe olivine, along with the presence of homogeneously nucleated lamellae showing only small differences in composition, imply that the exsolution has occurred during slow, continuous cooling at temperatures close to that of the crest of a coherent solvus dome. Although the real temperature of the exsolution is unknown, a lower limit can be estimated on the basis of the wavelength of the spinodal structure, the exsolution time, and diffusion rates measured at different temperatures (13). Using an observed wavelength of 5 μm and very conservative values for the other two parameters [a time of 4.5 billion years, equal to the age of the solar system; and the fastest Fe-Mg interdiffusion rate in olivine measured so far (14, 15)] gives a minimum temperature for the coherent solvus of $\sim 150^\circ\text{C}$. This estimate is very approximate because the value of a diffu-

Table 1. Chemical variability among lamellar olivines (Fa, mol%).

Grain	Minimum Fa	Maximum Fa	Range
1	24.6	27.9	3.3
3	25.6	28.9	3.3
5	22.8	27.1	4.3
5A	24.3	28.3	4.0
5B	25.7	27.2	2.5
6	25.3	29.1	3.8
6A	25.2	27.3	2.1
11	24.2	26.9	2.7

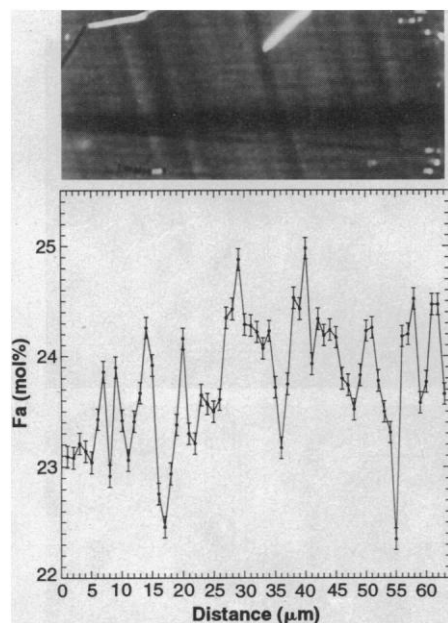


Fig. 2. Variation of fayalite content in olivine with distance in the grain whose BSE image is shown above it. White, troilite; light gray, Fe-rich lamellae; dark gray, Fe-poor lamellae. The black horizontal strip is the probe trace. The compositional variations approximate a sine wave, with maxima and minima exactly corresponding to the light and dark lamellae and a wavelength varying from a few to $\sim 5 \mu\text{m}$.

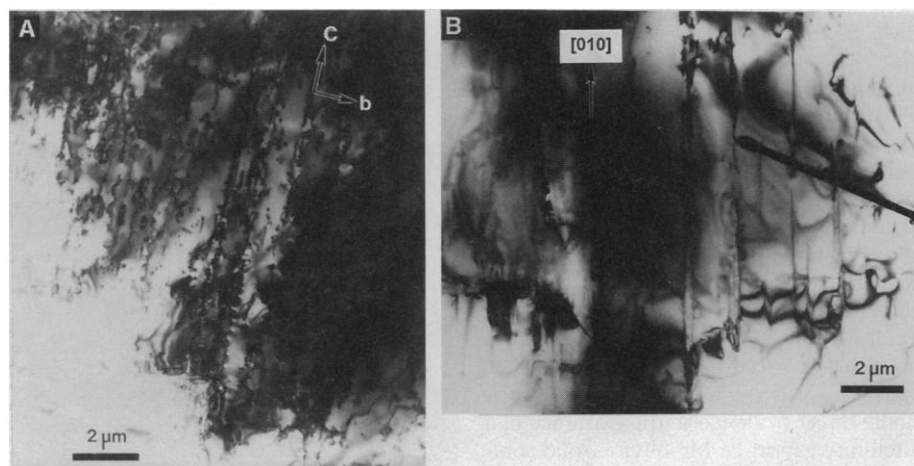


Fig. 3. Microstructures of olivine grains observed by TEM. (A) Grain #1. Narrow arrays of dislocations parallel the olivine *c* axis. These define the type of lamellar microstructure seen in transmitted light (Fig. 1B); however, no well-defined interfaces are present. (B) Distinct lamellar microstructure in olivine grain #3 with well-developed interfaces, which lie on (010). AEM analyses show that these interfaces represent the boundaries between Fe-rich and Fe-poor lamellae.

sion rate at low temperature, a key parameter, has been extrapolated from $\sim 1000^\circ\text{C}$ (14). A decrease in either the diffusion rate or the exsolution time would increase the minimum temperature of the solvus.

Thus, the exsolution lamellae in Divnoe olivines are consistent with a miscibility gap in Fe-Mg olivine at temperatures higher than $\sim 150^\circ\text{C}$. Among known models of olivine solid solutions only that of Sack and Ghiorso is consistent with this limit. In this model (6), equilibrium requires that homogeneous Divnoe olivines should exsolve into two phases with different compositions— Fa_{20-25} and Fa_{75-80} —below $\sim 300^\circ\text{C}$, or at a lower temperature if strain and surface energies are taken into account. At temperatures $< 200^\circ\text{C}$, a spontaneous spinodal decomposition can occur. At the higher exsolution temperatures predicted by the model of (6), the time required for exsolution would be reduced to more realistic values. The major discrepancy between our data and the model of (6) is the compositional difference between lamellae. If the lamellae in Divnoe olivines are equilibrated, as their compositions indicate, then the small compositional differences between lamellae and their positions on the Mg-rich side of the diagram may define the crest of an asymmetric solvus dome rather than the idealized symmetric solvus proposed by (6). An asymmetric olivine solvus has been suggested (4, 5, 7, 16), but all models predict its maximum at Fe-rich rather than Mg-rich compositions. Our data strongly suggest a solvus crest at around Fa_{26} , which is in agreement with experimental data by Schulien (17), who found compositionally different olivines (Fa_{28} and Fa_{49} at 420°C , Fa_{17} and Fa_{57} at 400°C) coexisting with aqueous solutions of $(\text{Fe,Mg})\text{Cl}_2$. If Schulien's data are correct, then the temperature of the solvus crest could be as high as $\sim 450^\circ\text{C}$, and exsolved olivine grains may be found in some meteorites and terrestrial basic plutons that experienced very slow cooling.

REFERENCES AND NOTES

1. W. A. Deer et al., *Rock-forming Minerals*, vol. 1A, *Orthosilicates* (Longman, London, 1982).
2. G. E. Brown Jr., in *Orthosilicates*, P. H. Ribbe, Ed., vol. 5 of *Reviews in Mineralogy* (Mineralogical Society of America, Washington, DC, ed. 2, 1982), pp. 275–392.
3. R. H. Nafziger and A. Muan, *Am. Mineral.* **52**, 1364 (1967).
4. K. Kitayama and T. Katsura, *Bull. Chem. Soc. Jpn.* **41**, 1146 (1968).
5. B. J. Wood and O. J. Kleppa, *Geochim. Cosmochim. Acta* **45**, 529 (1981).
6. R. O. Sack and M. S. Ghiorso, *Contrib. Mineral. Petrol.* **102**, 41 (1989).
7. N. M. Wiser and B. J. Wood, *ibid.* **108**, 146 (1991).
8. M. I. Petaev et al., *Meteoritics* **29**, 182 (1994).
9. M. I. Petaev, *Lunar Planet. Sci.* **24**, 1127 (1993).
10. Back-scattered electron images were obtained on a JEOL 733 Superprobe operating at 15 kV with a 20-nA beam current. Routine electron microprobe

analyses were performed at the same conditions with a spatial resolution of $\sim 3\ \mu\text{m}$ defined as the diameter of the electron interaction hemispheric volume (18). Fine-scale probing was done on the same instrument at an accelerating voltage of 10 kV, with spatial resolution of $\sim 1.5\ \mu\text{m}$. Transmission electron microscopy was performed on ion-milled samples of olivine that had been previously characterized by electron microprobe and BSE analysis. A JEOL 2000FX analytical transmission electron microscope operating at 200 kV was used throughout. In situ quantitative analyses were obtained through use of a Tracor Northern TN 5500 EDS system with a Be-window detector.

11. M. I. Petaev and A. J. Brearley, *Lunar Planet. Sci.* **25**, 1069 (1994).
12. I. Parsons and W. L. Brown, in *Diffusion, Atomic Ordering and Mass Transport*, J. Ganguly, Ed. (Springer-Verlag, New York, 1991), pp. 304–344; A. Putnis, *Introduction to Mineral Sciences* (Cambridge Univ. Press, New York, 1992).
13. The wavelength (λ) of a spinodal structure, the time (τ) needed to produce it, and the diffusion rate (D_i) are related by the equation $\lambda^2 = \tau D_i$ (19). Variations of the diffusion rate with temperature are described

by the equation $D_i = 9.6 \times 10^{-9} \exp(-15888/T)$, which is derived from experimental data (14) corrected for compositional and redox differences.

14. D. K. Buening and P. R. Buseck, *J. Geophys. Res.* **78**, 6852 (1973).
15. M. Morioka and H. Nagasawa, in *Diffusion, Atomic Ordering and Mass Transport*, J. Ganguly, Ed. (Springer-Verlag, New York, 1991), pp. 176–197.
16. R. J. Williams, *Earth Planet. Sci. Lett.* **15**, 296 (1972).
17. S. Schulien, *Contrib. Mineral. Petrol.* **74**, 85 (1980). Estimates of olivine compositions were based on x-ray diffraction patterns with an accuracy of 5% in the most favorable conditions.
18. J. I. Goldstein et al., *Scanning Electron Microscopy and X-ray Microanalysis* (Plenum, New York, 1981).
19. J. W. Cahn, *Trans. Metall. Soc. AIME* **242**, 166 (1968).
20. We thank NASA for financial support (grants NAGW-3451 to J.A.W. and NAGW-3347 to J.J.P.). Transmission electron microscopy was carried out in the Electron Microbeam Analysis Facility, Department of Earth and Planetary Sciences and Institute of Meteoritics, University of New Mexico.

2 June 1994; accepted 28 September 1994

Teleseismic Search for Slow Precursors to Large Earthquakes

Pierre F. Ihmlé and Thomas H. Jordan*

Some large earthquakes display low-frequency seismic anomalies that are best explained by episodes of slow, smooth deformation immediately before their high-frequency origin times. Analysis of the low-frequency spectra of 107 shallow-focus earthquakes revealed 20 events that had slow precursors (95 percent confidence level); 19 were slow earthquakes associated with the ocean ridge–transform system, and 1 was a slow earthquake on an intracontinental transform fault in the East African Rift system. These anomalous earthquakes appear to be compound events, each comprising one or more ordinary (fast) ruptures in the shallow seismogenic zone initiated by a precursory slow event in the adjacent or subjacent lithosphere.

Low-frequency teleseismic signals contain information about earthquake rupture processes that is crucial to understanding large earthquakes of long duration. Standard waveform-modeling procedures poorly constrain the source spectrum below about 7 to 10 mHz, but newer techniques, based on the averaging of amplitude and phase-delay measurements over global networks of high-performance stations, yield good spectral resolution at seismic frequencies as low as 1 mHz (1). We recently synthesized the spectrum of the great Macquarie Ridge earthquake (23 May 1989) from 1 to 50 mHz from overlapping sets of free-oscillation, surface-wave, and body-wave measurements. We inferred from a series of spectral inversions that the main shock was initiated by a slow, smooth precursor that began several hundred seconds before the high-frequency origin time (1). Slow precursors

large enough to be teleseismically detectable have been found for other large earthquakes in oceanic lithosphere, including the great Chilean earthquake of 22 May 1960 (2), the intermediate-focus Peru-Ecuador event of 12 April 1983 (3), and some slow earthquakes on the ocean ridge–transform system (4).

One can detect a slow precursor by comparing the origin time of an earthquake determined from high-frequency waves with an upper bound on its start time inferred from low-frequency waves (3). We used this approach to investigate three groups of shallow-focus earthquakes (Fig. 1). Group A is a set of 68 events associated with the ocean ridge–transform system, comprising essentially all of the well-recorded, large (moment magnitude $M_w \geq 6.4$) earthquakes on or near mid-ocean ridge segments and oceanic transform faults between 1977 and 1992 (5). Group B is a sample of 23 earthquakes in zones of plate convergence, including 6 predominantly strike-slip events in volcanic arcs and back-arc basins. Group C comprises 1 normal, 11 strike-slip, and 4 reverse-faulting events

P. F. Ihmlé, Institut de Physique du Globe, 4 Place Jussieu, Paris Cedex 75252, France.
T. H. Jordan, Department of Earth, Atmospheric, and Planetary Sciences, Massachusetts Institute of Technology, Cambridge, MA 02139, USA.

*To whom correspondence should be addressed.